Oncogene (2011) 1–11

www.nature.com/onc

ORIGINAL ARTICLE

Insulin-like growth factor binding protein 5 suppresses tumor growth and metastasis of human osteosarcoma

Y Su[1,2,3,8], ER Wagner[2,8], Q Luo[1,2,3], J Huang[2,3], L Chen[2,3], B-C He[2,3], G-W Zuo[2,3], Q Shi[2,3], B-Q Zhang[2,3], G Zhu[1,2,3], Y Bi[1,2,3], J Luo[2,3], X Luo[2,3], SH Kim[2], J Shen[2], F Rastegar[2], E Huang[2,4], Y Gao[2,5], J-L Gao[2], K Yang[2,6], C Wietholt[7], M Li[1,3], J Qin[1,2,3], RC Haydon[2], T-C He[1,2,3] and HH Luu[2]

[1]Stem Cell Biology and Therapy Laboratory, The Children's Hospital of Chongqing Medical University, Chongqing, China; [2]Department of Surgery, The University of Chicago Medical Center, Chicago, IL, USA; [3]Key Laboratory of Diagnostic Medicine Designated by Chinese Ministry of Education and the Affiliated Hospitals of Chongqing Medical University, Chongqing, China; [4]School of Bioengineering, Chongqing University, Chongqing, China; [5]Department of Geriatrics, Xinhua Hospital of Shanghai Jiatong University, Shanghai, China; [6]Department of Cell Biology, The Third Military Medical University, Chongqing, China and [7]Department of Radiology, The University of Chicago Medical Center, Chicago, IL, USA

Osteosarcoma (OS) is the most common primary malignancy of bone. There is a critical need to identify the events that lead to the poorly understood mechanism of OS development and metastasis. The goal of this investigation is to identify and characterize a novel marker of OS progression. We have established and characterized a highly metastatic OS subline that is derived from the less metastatic human MG63 line through serial passages in nude mice via intratibial injections. Microarray analysis of the parental MG63, the highly metastatic MG63.2 subline, as well as the corresponding primary tumors and pulmonary metastases revealed insulin-like growth factor binding protein 5 (IGFBP5) to be one of the significantly downregulated genes in the metastatic subline. Confirmatory quantitative RT–PCR on 20 genes of interest demonstrated IGFBP5 to be the most differentially expressed and was therefore chosen to be one of the genes for further investigation. Adenoviral mediated overexpression and knockdown of IGFBP5 in the MG63 and MG63.2 cell lines, as well as other OS lines (143B and MNNG/HOS) that are independent of our MG63 lines, were employed to examine the role of IGFBP5. We found that overexpression of IGFBP5 inhibited *in vitro* cell proliferation, migration and invasion of OS cells. Additionally, IGFBP5 overexpression promoted apoptosis and cell cycle arrest in the G1 phase. In an orthotopic xenograft animal model, overexpression of IGFBP5 inhibited OS tumor growth and pulmonary metastases. Conversely, siRNA-mediated knockdown of IGFBP5 promoted OS tumor growth and pulmonary metastases *in vivo*. Immunohistochemical staining of patient-matched primary and metastatic OS samples demonstrated decreased IGFBP5 expression in the metastases. These results suggest 1) a role for IGFBP5 as a novel marker that has an important role in the pathogenesis of OS, and 2) that the loss of IGFBP5 function may contribute to more metastatic phenotypes in OS.
Oncogene advance online publication, 4 April 2011; doi:10.1038/onc.2011.97

Keywords: osteosarcoma; tumorigenesis; metastasis; IGFBP5; animal model

Introduction

Osteosarcoma (OS) is the most common primary malignancy of bone in children and young adults (Whelan, 1997). The genetic events that lead to the development and metastasis of OS are not known and may be a reflection of the complexity of OS (Letson and Muro-Cacho, 2001; Fuchs and Pritchard, 2002; Ragland *et al*., 2002). Although approximately 80% of OS patients have metastatic disease at the time of diagnosis, only 10–15% of these lesions are detectable with current radiographic imaging modalities (Yonemoto *et al*., 1998; Kaste *et al*., 1999). Therefore, there is a clinical need to identify genetic markers that not only provide insight into the pathogenesis of OS, but also its metastasis. With the current treatment for OS, which includes wide resection and chemotherapy, the average 5-year disease-free survival rate is 65–70% (Davis *et al*., 1994; Mankin *et al*., 2004). However, despite advances in chemotherapy and surgical techniques over the last three decades, there has not been any significant improvement in patient survival. Although some genetic or hereditary abnormalities are associated with OS, the events that lead to the development and metastasis of OS are poorly understood.

We have recently established a highly tumorigenic and metastatic human OS cell line that has not been

Correspondence: Dr HH Luu, Suzanne Berman Oncology Laboratory, Department of Surgery, The University of Chicago Medical Center, 5841 South Maryland Avenue, MC3079, Chicago, IL 60637, USA.
E-mail: hluu@surgery.bsd.uchicago.edu
[8]These authors contributed equally to this work.
Received 24 June 2010; revised 6 February 2011; accepted 27 February 2011

transformed exogenously (Su *et al*., 2009). Although the parental line (MG63) formed small tumors and occasional metastases in an orthotopic xenograft model, we re-passaged the occasional metastases through the athymic nude mice until a highly metastatic line (MG63.2) was established. The MG63.2 cell line demonstrated greater migratory and invasive potential *in vitro*, along with larger tumors and more pulmonary metastases *in vivo*. In this report, we conducted microarray analyses and compared the expression profiles between the parental MG63 and the highly metastatic MG63.2 subline. Among the genes that were most significantly differentially expressed, we found that insulin-like growth factor binding protein 5 (IGFBP5) had a 10-fold higher expression in the parental MG63 cell line. IGFBP5 is a member of the IGFBP family of six secreted proteins that are involved in the regulation of the mitogens IGF I and II, via complex receptor and protease interactions (Rosenzweig, 2004). IGFBPs have an important role in a variety of pathologic and physiologic pathways, such as mesenchymal progenitor cell proliferation, differentiation and migration (Schneider *et al*., 2002).

In this investigation, we examined the role of IGFBP5 in OS pathogenesis and metastasis. On the basis of our microarray data, we hypothesized that IGFBP5 inhibits tumor growth and metastasis in OS. We found that overexpression of IGFBP5 inhibited cell proliferation, migration and invasion, whereas promoting apoptosis, in OS cell lines. Overexpression of IGFBP5 inhibited OS tumor growth and lung metastasis *in vivo*. Conversely, siRNA knockdown of IGFBP5 promoted OS tumor growth and lung metastasis *in vivo*. Furthermore, IGFPBP5 expression is decreased in metastatic lesions when compared with the primary tumors in patients.

Results

Lower IGFBP5 expression in the highly metastatic MG63.2 and 143B lines

We have recently established a highly metastatic subline (MG63.2) from the parental MG63 cell line. In this study, we sought to examine the expression profiles of these two lines with a similar genetic background. RNA was collected from the MG63 and MG63.2 cell lines, MG63 and MG63.2 primary tumors, as well as lung metastases from the MG63.2 injected animals. Genes on the Affymetric chip (Affymetric, Santa Clara, CA, USA) were evaluated and the filter for differentially expressed genes set at a greater than two-fold change in expression and a P-value <0.05. In this experiment, we identified 200 genes that were most differentially expressed and then performed a DNA-Chip cluster analysis. Hierarchical cluster analysis is commonly used to create a group of genes that have similar patterns of expression. As shown in Figure 1, the upregulated and downregulated genes cluster together among the metastatic MG63.2 and MG63.1 (MG63.2's immediate predecessor in the passaging process) cell lines, primary tumors and lung metastases.

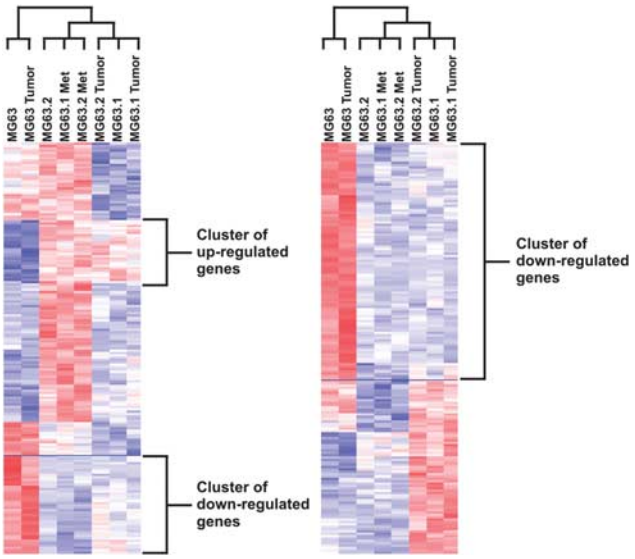

Figure 1 Microarray and hierarchal cluster analyses of the top 200 differentially expressed genes between x and y. The top 200 differentially expressed genes from the microarray analysis using total RNA isolated from MG63, MG63.1 and MG63.2 cells, and tumors, as well as lung metastases (Met) from the MG63.1 and MG63.2 animals were analyzed using dChip hierarchal clustering analysis. A large number of genes show distinct expression patterns between x and y. The colors indicate the relative gene expression level within the gene across all samples. Red: high expression; blue: low expression. See Materials and methods for details.

The metastatic lesions demonstrate a closer hierarchical relationship with that of MG63.2 subline. This is in comparison with the parental MG63 cell line and MG63 tumor, which are closely related. Examples of the most differentially expressed genes and their reported functions are shown in Table 1. We selected 20 differentially expressed genes of interest on the basis of their known functions and determined the expression levels by quantitative real-time RT–PCR. Our confirmatory RT–PCR among these 20 genes demonstrated IGFBP5 to be most differentially expressed. Thus, we chose to focus on IGFBP5 in current study, whereas other candidates are being investigated as separate studies.

On the basis of the microarray analysis, there was a 10-fold decrease in expression in IGFBP5 between the MG63 and MG63.2 lines. By quantitative PCR, there was greater than a 30-fold decrease in IGFBP5 expression in the highly metastatic MG63.2 tumor or MG63.2 lung metastasis versus the parental MG63 tumor (P-value <0.001) (Figure 2a). To assure that this finding is not specific to only the MG63-derived sublines, we examined IGFBP5 expression in two other commonly used OS cell lines (143B and MNNG/HOS) that are not related to the MG63 lines (Figure 2b). We have previously shown that the 143B line is significantly more metastatic compared with the MNNG/HOS line (Luu *et al*., 2005a; Su *et al*., 2009). IGFBP5 mRNA and protein expression was detectable among the lines, with MNNG/HOS demonstrating the higher expression compared with the highly metastatic 143B line. As expected, the MG63.2 line had lower expression compared with the parental MG63 line.

Table 1 Micrroarray results

Gene	*Accession number*	*FOC*	*Function(s)*
Top upregulated genes			
Interferon stimulated gene 20 kDa	NM_002201	32.03	Exonuclease, immune modulator
SLC6A15	NM_018057	31.03	Neutral amino acid transporter
Coagulation factor III	NM_001993	21.04	Coagulation pathway
EST	AA156240	19.74	Unknown
c10orf10	AL136653	17.1	Unknown, induced by fasting and progesterone
TFPI2	AL574096	14.89	Potential tumor suppressor
Dual specificity phosphatase 4	BC002671	14.67	Negative regulator of MAPK pathway
Frizzled homolog 8	AL121749	14.39	Wnt signaling
RGM domain family, member B	BE206621	14.08	Nervous system development, BMP signaling
EST	BE877420	13.53	Unknown
EST	BE222344	12.93	Unknown
HMGA2	NM_003483	12.07	Transcription factor, growth and differentiation
HBEGF	NM_001945	11.6	Growth factor
SPOC domain containing 1	BF689253	11.2	Unknown
Carbonic anhydrase IX/CA9	NM_001216	10.91	Regulator of tumor pH, target of HIF
Top downregulated genes			
IGFBP5	AW007532	−10.93	Modulator of growth and differentiation in IGF pathway
SERPINI1	NM_005025	−11.33	Serine proteinase inhibitor
GIT2	AF124491	−11.35	Signal transduction
CCDC80	AA570507	−11.53	Adipogenesis
Osteoglycin (mimecan)	NM_014057	−12.94	Osteoinductive factor, growth factor
S100 A5	NM_002962	−14.2	E-F hand calcium binding protein,
EST	AW299568	−14.38	Unknown
Brother of CDO/BOC	W72626	−14.71	Mesenchymal cell differentiation
Matrilin 2	NM_002380	−15.43	Extracellular matrix assembly
Myocilin	D88214	−18.39	Cytoskeletal function
NESH binding protein/NeshBP	AB056106	−19.9	Interacts with ABI family of tyrosine kinases
Periostin, osteoblast specific factor	D13665	−22.41	Osteoblastic differentiation
Microfibrillar-associated protein 4	R72286	−23.62	Assembly of extracellular matrix fibers
Complement factor H	X04697	−29.36	Complement activation
Trophinin/trophinin	AF349719	−39.04	Apical cell adhesion in embryogenesis

Abbreviation: FOC, fold of change.

Decreased IGFBP5 expression in pulmonary metastases
We next examined the expression of IGFBP5 by immunohistochemistry in clinical specimens. Searching our pathology database, we identified 25 patients who had pulmonary metastatic lesions excised, and the paraffin blocks were available at our institution. Among these 25 patients, 14 had matched-primary specimens whereas 11 did not have a primary tumor sample at our institution. Often, patients are referred to our institution after the biopsy is done elsewhere. We found that expression of IGFBP5 was consistently decreased in the metastatic lesions compared with the primary tumors (Table 2). Figure 2c is an example of a primary lesion that had strong staining for IGFBP5, whereas the matched-metastatic lesion had none. For both the patient, unmatched and matched samples, the mean immunohistochemical score for the primary lesions was 2.5, compared with 1.0 for the metastatic lesions (P-values 0.0012 and <0.0001, respectively). These results suggest that IGFBP5 expression is lost when OS metastasizes.

IGFBP5 inhibits proliferation, migration and invasion
Our microarray, confirmatory RT–PCR and immunohistochemical data support our hypothesis that IGFBP5 may be involved in inhibiting metastasis and tumor growth in human OS. To test this hypothesis, we next characterized the role of IGFBP5 on cell proliferation, migration and invasion by using adenoviral vectors to overexpress or knock down endogenous IGFBP5. As shown in Figure 2d (upper panel), we were able to knock down endogenous IGFBP5 expression in our OS cell lines, as detected by RT–PCR and western blot analysis. We also tested the scrambled siRNA control and showed no difference with the red fluorescence protein (RFP) control (data not shown). Overexpression of IGFBP5 by adenoviral transduction was detectable by western blot analysis in HEK293 cells, which have very low endogenous IGFBP5 expression (Figure 2d, lower panel).

We next assessed the effects of IGFBP5 on phenotypes important for metastasis and tumor growth. As demonstrated in Figures 3a and b, IGFBP5 overexpression inhibited cell proliferation, whereas knockdown promoted cell proliferation (all P-values $\leqslant 0.05$). Specifically, the doubling times in hours for the MG63.2-expressing RFP, IGFBP5 and siIGFBP5 are 21.0 ± 0.5, 22.8 ± 0.3 and 20.0 ± 0.3, respectively, and for the 143B cells are 18.0 ± 0.8, 19.8 ± 0.7 and 16.6 ± 0.6, respectively. Similar results were seen in parental MG63 and MNNG/HOS cell lines, as well as the scrambled siRNA and RFP controls (data not shown). Next, we examined the effects of IGFBP5 overexpression and siRNA-mediated knockdown on OS cell migration. We found that overexpression of IGFBP5 inhibited the

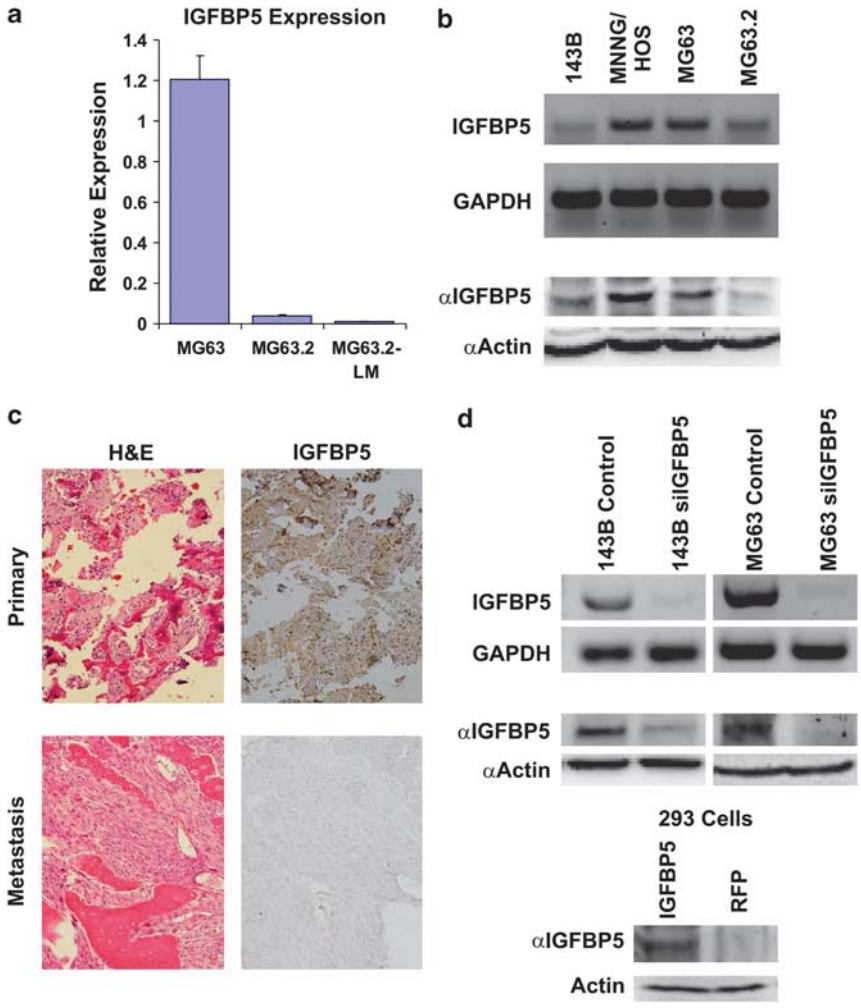

Figure 2 IGFBP5 expression in tumor samples and cell lines. (**a**) Quantitative real-time RT–PCR on the parental MG63 tumor, highly metastatic MG63.2 tumor and a lung metastasis from an MG63.2 injected animal is shown. (**b**) Endogenous expression of IGFBP5 analyzed via semi-quantitative RT–PCR and western blot in four commonly used OS cell lines. GAPDH and anti-actin are controls for the RT–PCR and western blot, respectively. (**c**) Example of the loss of IGFBP5 immunohistochemical staining of a pulmonary metastatic lesion, when compared with the matched primary lesion (magnification $\times 200$). Note the loss of IGFBP5 staining intensity in the metastatic lesion. Malignant osteoid production is present in both the primary and metastatic lesions. (**d**) Knockdown and overexpression of IGFBP5. IGFBP5 knockdown demonstrated by semi-quanitative RT–PCR and western blot analysis (upper panel). GAPDH and anti-actin are controls for the RT–PCR and western blot, respectively. Western blot analysis of IGFBP5 adenoviral overexpression in 293 cells, which has low endogenous IGFBP5 expression (lower panel).

ability of MG63.2 cells to close a gap in a wound healing assay (Figure 3c). Conversely, knockdown of IGFBP5 enhanced the MG63.2 cells' ability to migrate in the assay. Similar results were seen with the parental MG63, MNNG/HOS and 143B cell lines, as well as the scrambled siRNA and RFP controls (data not shown). Finally, we used a Matrigel invasion assay to analyze the role of IGFBP5 on the OS cell's invasive potential. As shown in Figure 3d, we found that overexpression of IGFBP5 decreased invasion by 55%, whereas siRNA-mediated knockdown increased invasion by 110% in the MG63.2 cells, when compared with the control RFP control group, P-value <0.001. Similar results were seen in the parental MG63, MNNG/HOS and 143B cell lines (data not shown).

IGFBP5 inhibits primary tumor growth

We next sought to investigate IGFBP5's role on primary tumor growth in our orthotopic animal model, using the MG63.2 and 143B cell lines that we have previously characterized (Luu *et al*., 2005a; Su *et al*., 2009). Cells were equally infected with adenovirus expressing RFP only (AdRFP), AdR-IGFBP5 or AdR-siIGFBP before subperiosteal implantation. As seen in Figure 4a, overexpression of IGFBP5 by adenoviral transduction in the 143B cell line led to a decrease in primary tumor growth compared with the RFP control. Consistent with our overexpression data, siRNA-mediated knockdown of endogenous IGFBP5 resulted in an increase in tumor growth (Figure 4a). Overexpression of IGFBP5 increased the doubling time in the 143B and MG63.2 cells by

Table 2 Immunohistochemical scores of primary tumors and pulmonary metastases

Patient #	*Age*	*Gender*	*Location*	*Immunohistochemical Score*	
				Primary	*Metastasis*
1	14	F	Tibia	2	1
2	16	F	Femur	No sample	1
3	18	M	Humerus	3	1
4	13	F	Tibia	3	1
5	16	M	Tibia	3	0
6	14	M	Femur	No sample	1
7	17	M	Femur	No sample	1
8	11	M	Femur	1	0
9	12	M	Femur	No sample	2
10	15	F	Tibia	No sample	1
11	34	M	Femur	No sample	0
12	31	F	Tibia	2	1
13	16	F	Humerus	2	1
14	15	M	Scapula	3	1
15	13	M	Humerus	3	1
16	16	M	Tibia	1	1
17	13	M	Femur	No sample	2
18	13	M	Tibia	3	1
19	18	F	Humerus	No sample	2
20	12	F	Femur	No sample	1
21	16	M	Femur	No sample	2
22	11	F	Femur	No sample	1
23	16	M	Tibia	2	2
24	22	M	Femur	3	0
25	13	F	Femur	3	1

No sample: indicates no paraffin blocks for the primary tumor at our institution. *P*-value 0.0012 and <0.0001 for unmatched and matched samples, respectively.

137 and 89%, respectively, when compared with the RFP control group (*P*-values $= 0.04$ and 0.02, respectively). Specifically, the doubling times for the IGFBP5 overexpression, IGFBP5 knockdown and RFP control were 10.2 ± 4.3 days, 3.2 ± 1.9 days and 4.3 ± 1.2 days, respectively, in the 143B injected animals. Similar results were seen in the MG63.2 cell line (Figure 4b). The doubling times for the IGFBP5 overexpression, IGFBP5 knockdown and RFP control were 44.5 ± 15.2 days, 17.8 ± 6.5 days and 23.5 ± 9.8 days, respectively, in the MG63.2 injected animals.

When the primary 143B tumors were grossly visualized, there was a clear difference in tumor size between the IGFBP5, RFP and siIGFBP5 groups (Figure 4c, top row). Furthermore, live animal bioluminescent imaging demonstrated the difference in primary tumor sizes between the three groups (Figure 4c, middle row). By the second week, there was consistently increased luciferase activity in the siIGFBP5 and a remarkable decrease in the IGFBP5 group, compared with the RFP control. MicroCT analysis demonstrated destruction of the proximal tibia when IGFBP5 was knocked down (Figure 4c, bottom row). The tibias of the mice in the IGFBP5 overexpression group remained relatively intact. Random sections dividing the tibia and tumors sagitally were then stained with hematoxylin and eosin. The RFP and knockdown groups had destruction and invasion through the posterior cortex and into the marrow, whereas the tumors in the IGFBP5 overexpression group had less apparent cortical destruction and invasion (Figure 4d). Similar results were seen in the MG63.2 tumors (data not shown).

IGFBP5 inhibits spontaneous pulmonary metastasis

We next examined the role of IGFBP5 on spontaneous pulmonary metastases in an orthotopic xenograft model of OS using the MG63.2 and 143B cell lines that we have previously characterized (Luu *et al*., 2005a; Su *et al*., 2009). Again the cells were stably tagged with luciferase for weekly Xenogen bioluminescent imaging. Pulmonary metastases were easily detected when endogenous expression of IGFBP5 was knocked down in the MG63.2 cell lines (Figure 5a, top row). This was grossly apparent in the lungs harvested from the animals (Figure 5a, middle row). Overexpression of IGFBP5 inhibited pulmonary metastasis. In some animals in the knockdown group, the pulmonary metastases were so large that they became adherent to the chest wall. Similar results were seen in the 143B animals, but with higher efficiency of metastasis (data not shown).

Next, the lungs were subjected to histologic evaluation to compare the difference in microscopic metastases. Random sections at the maximal width of the lungs were stained with hematoxylin and eosin, as shown in Figure 5a, bottom row. In the RFP control for the MG63.2 animals, some micro-metastases were seen. However, the tumor burden was not large enough to be detected by the bioluminescent imaging. All the lungs were scored for the presence or absence of metastases (Figure 5b). Knockdown of IGFBP5 resulted in a significantly increased incidence of pulmonary metastasis, whereas overexpression resulted in suppression. When taken together for 143B and MG63.2 cell lines, 10/10 animals in the siIGFBP5 group had metastasis, whereas 5/10 RFP animals and 1/10 IGFBP5 animals had metastases (*P*-values <0.0001 and 0.032 for MG63.2 and 143B, respectively). Overall, our pulmonary evaluations demonstrated that IGFBP5 overexpression suppressed, whereas IGFBP5 knockdown promoted, OS metastasis.

IGFBP5 inhibits proliferation and promotes apoptosis

To examine the mechanism underlying the suppression of tumor growth by IGFBP5, we evaluated for the presence of a late apoptotic marker, cleaved caspase-3 and performed a cell cycle and proliferation analysis. As shown in Figure 6a, overexpression of IGFBP5 led to a marked increase in caspase-3 expression as compared with the RFP control or knockdown groups in both MG63.2 and 143B cell lines. Immunohistochemical staining with an anti-cleaved caspase-3 antibody revealed a similar increase in the overexpression group in both cell lines as depicted in Figure 6b for the 143B cells. Next, flow cytometry was used to sort the 143B and MG63.2 cells to determine the percentage of cells undergoing apoptosis and in each stage of the cell cycle. Overexpression of IGFBP5 increased the number of cells in the early apoptotic phase by over three-fold, from 4.13 to 14.80%, and late apoptotic markers by

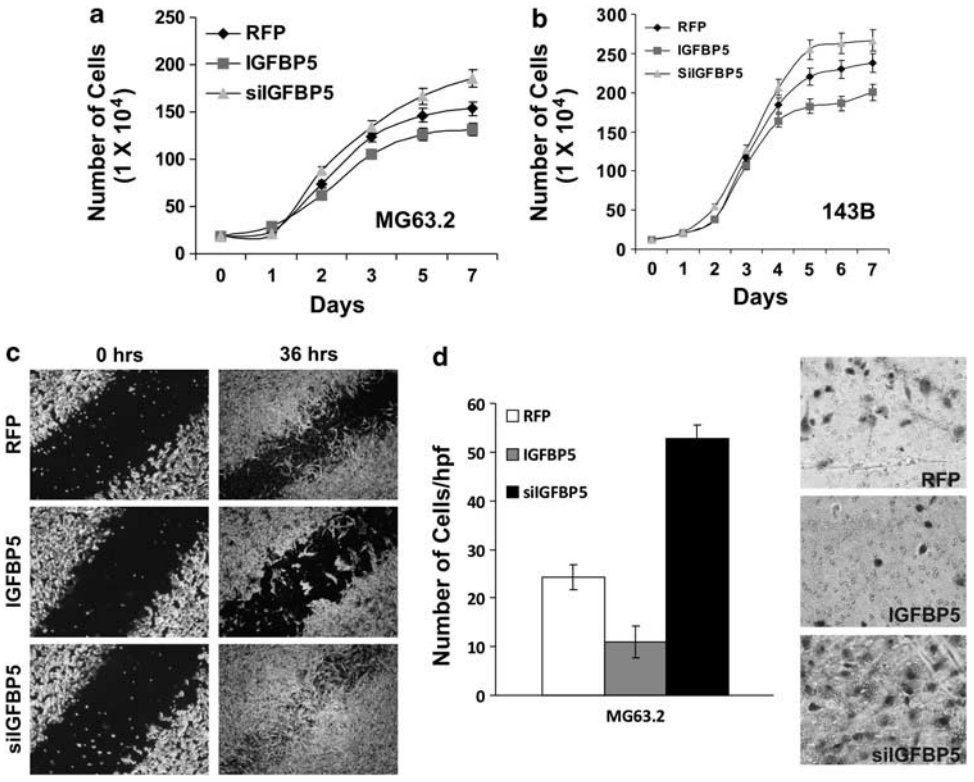

Figure 3 IGFBP5 inhibits cell proliferation, migration and invasion. (**a**, **b**) *In vitro* cell proliferation assayed by cell counting for the MG63.2 and 143B cell lines expressing IGFBP5, siIGFBP5 and RFP control are shown. (**c**) Cell migration in a wound-healing assay. Images taken at 0 and 36 h for the MG63.2 cell line are shown and depict the ability of the cells to migrate across the gap for each group. (**d**) Cell invasion. 1×10^5 MG63.2 cells expressing IGFBP5, siIGFBP5 or RFP control were plated on the upper chamber of a Transwell unit coated with Matrigel. Fetal calf serum was used as a chemoattractrant in the lower chamber. The number of invaded cells per hpf is graphed. Representative images for each treatment group are shown.

two-fold, from 2.13 to 4.45% (Figure 6c) in the MG63.2 cell line, with similar results in the 143B cell line. Averaged among the lines, overexpression of IGFBP5 led to a significantly increased number of cells in the G1 phase of the cell cycle versus the RFP control (Figure 6d), 55.9 versus 46.7%, respectively (P-value = 0.04). IGFBP5 knockdown decreased the number of cells in the G1 phase to 43.1% from 46.7% in the RFP control (P-value = 0.04). Taken together, these results indicate that IGFBP5 overexpression promotes apoptosis and maintains a greater proportion of cells in G1 phase of the cell cycle, thereby inhibiting tumor growth.

Discussion

We previously reported on the identification and characterization of a highly metastatic and tumorigenic OS cell line (MG63.2), from the marginally metastatic parental MG63 line (Su *et al*., 2009). Microarray analysis revealed a 10-fold decrease in IGFBP5 expression in the highly metastatic MG63.2 line, compared with the parental MG63 line. We characterized the function of IGFBP5 in the MG63.2 cell line, as well as an independent OS cell line. From our data, we identified IGFBP5 as a novel gene regulating OS metastasis and tumor growth. Our data points to an inverse relationship between IGFBP5 expression and tumor growth, as well as metastatic potential. Of the four OS lines analyzed, the two lines with the highest proliferative, invasive and metastatic capabilities (143B and MG63.2) showed significantly lower IGFBP5 expression. Through overexpression and silencing experiments, we find that IGFBP5 inhibits cell proliferation, migration and invasion *in vitro*, as well as tumor growth and metastasis in an orthotopic xenograft model of human OS. Additionally, IGFBP5 expression is decreased in metastatic samples taken from OS patients, when compared with the primary tumors.

Although little is known about the role of IGFBP5 in OS, the IGF pathway has been implicated in a number of human cancers, including Ewing's sarcoma and OS (Manara *et al*., 2007; Avnet *et al*., 2009). The IGFBPs are associated with a variety of pathologic and physiologic pathways (Schneider *et al*., 2002). However, there is conflicting data on the relationship between IGFBP expression and human cancers. In fact, there are many cases where the same IGFBP has been shown to have both stimulatory, as well as inhibitory effects on tumorigenesis, depending on the tumor type (Mukherjee and Rotwein, 2007). For example, IGFBP5 has been shown to induce caspase expression and promote apoptosis in breast cancer (Butt *et al*., 2003; Butt *et al*., 2005). In contrast, IGFBP5 is believed to facilitate prostate

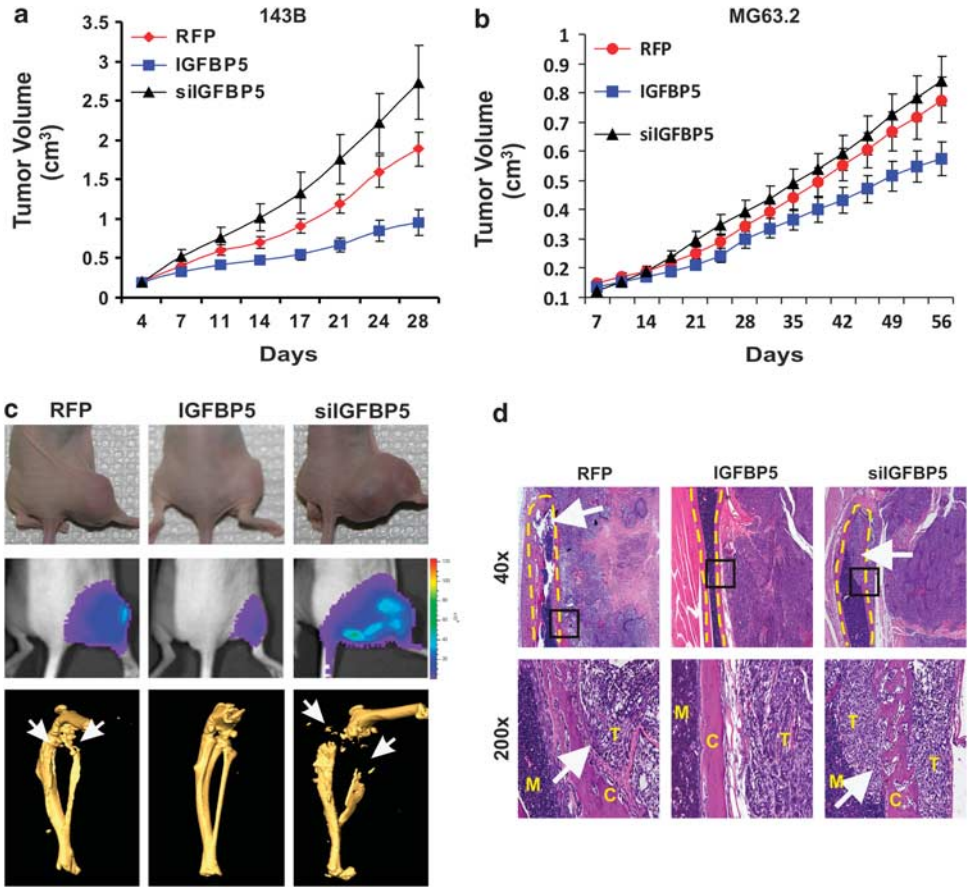

Figure 4 IGFBP5 suppresses primary tumor growth. (**a**, **b**) Primary tumor growth. 1.5×10^6 cells expressing IGFBP5, siIGFBP5 or RFP control are injected subperiosteally in the proximal posterior tibia of nude mice. The tumor volume for each treatment group in the 143B and MG63.2 injected animals is graphed. (**c**) Representative photo images (top row) and bioluminescent images (middle row) for each treatment group in the 143B injected animals at 4 weeks are shown. MicroCT images (bottom row) of tibias for each treatment group are shown. Note the significant bone destruction (arrows) in the siIGFBP5 and some in the RFP group (arrows). (**d**) Histology images demonstrate the degree of tumor invasion into the tibia of 143B-injected animals at the indicated magnification. The outline of tibial bone cortex is indicated (dashed lines). Note the bone destruction and tumor infiltration into bone in the siIGFBP5 and control RFP groups (arrows) at $\times 200$. M, marrow; T, tumor; C, cortical bone.

cancer metastasis (Xu *et al*., 2007). Additionally, IGFBP5 is downregulated in renal and cervical tumors, but appears to be upregulated in high-grade ovarian carcinoma and thyroid papillary carcinoma (Stolf *et al*., 2003; Cheung *et al*., 2005; Takahashi *et al*., 2005; Wang *et al*., 2006). These conflicting results may be due to IGFBP5 mediating its effects in both IGF-dependent and IGF-independent pathways (Akkiprik *et al*., 2008).

In our study, we find that IGFBP5 suppresses metastatic phenotypes in OS. These findings are supported by the reported functions of the three conserved domains of this protein, the N-terminal, C-terminal and L domains (Schneider *et al*., 2002; Akkiprik *et al*., 2008). In particular, the C-terminal domain might be involved in the inhibition of OS migration, invasion and metastasis. This domain has been shown to interact with extracellular matrix proteins, such as fibronectin, thrombospondin-1, osteopontin and vitronectin (Akkiprik *et al*., 2008). In addition, IGFBP5 contains a total of three heparin-binding motifs in the C-terminal and L domains (Song *et al*., 2001). These motifs in IGFBP5 bind to glycosaminoglycans in the extracellular matrix and can be blocked by heparin (Song *et al*., 2001). The ability of IGFBP5 to bind to extracellular matrix proteins may modulate cell–cell and cell–matrix interactions. The net potential effect is regulation of cell adhesion, migration and metastasis. Thus, our observed inhibitory effects of IGFBP5 on the metastatic phenotypes may potentially be regulated by the C-terminal and L domains of this protein.

Our observed inhibition of cell proliferation and tumor growth is supported by the reported functions of the N-terminal and C-terminal domains of IGFBP5. The N-terminal domain of IGFBP5 has been shown to bind to IGF, thereby regulating mitogenic activity (Akkiprik *et al*., 2008). Binding of IGFBP5 to IGF is believed to prevent or modulate IGF binding to the IGF receptor (Akkiprik *et al*., 2008). Additionally, the C-terminal domain of IGFBP5 contains a nuclear localization signal and might mediate the observed

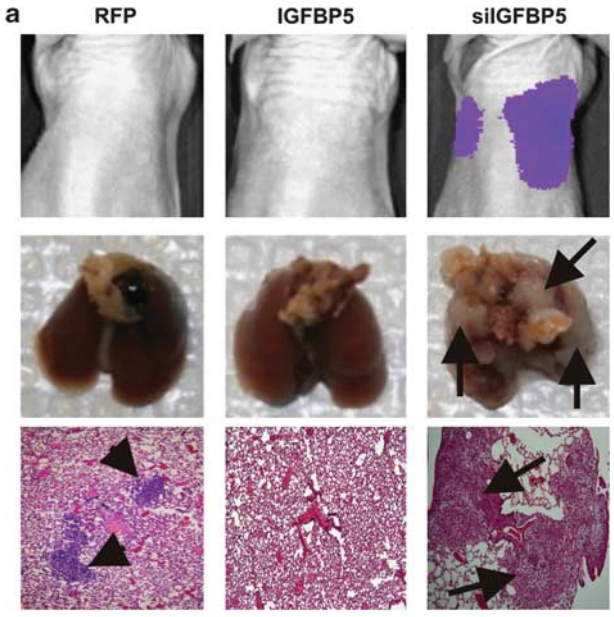

b

Group	No. of Animals with Metastases	
	MG63.2	143B
RFP	2/5	3/5
IGFBP5	0/5	1/5
siIGFBP5	5/5	5/5
χ^2 p-value	<.0001	0.032

Figure 5 IGFBP5 inhibits pulmonary metastasis. (**a**) Representative bioluminescent images (top row) of the mice in each treatment group at 8 weeks after 1.5×10^6 MG63.2 cells were injected subperiosteally into the proximal posterior tibia. Representative images of the harvested lungs from the MG63.2 injected animals are shown for each treatment group (middle row). Note the overt metastases (middle row) in the siIGFBP5 lung (arrows). Representative histologic sections (bottom row) of the lungs for each group are shown. Note the micro-metastases in the RFP group (arrowheads) and the large metastases in the siIGFBP6 group (arrows). (**b**) The number of animals with pulmonary metastases in both the 143B and MG63.2 treatment groups.

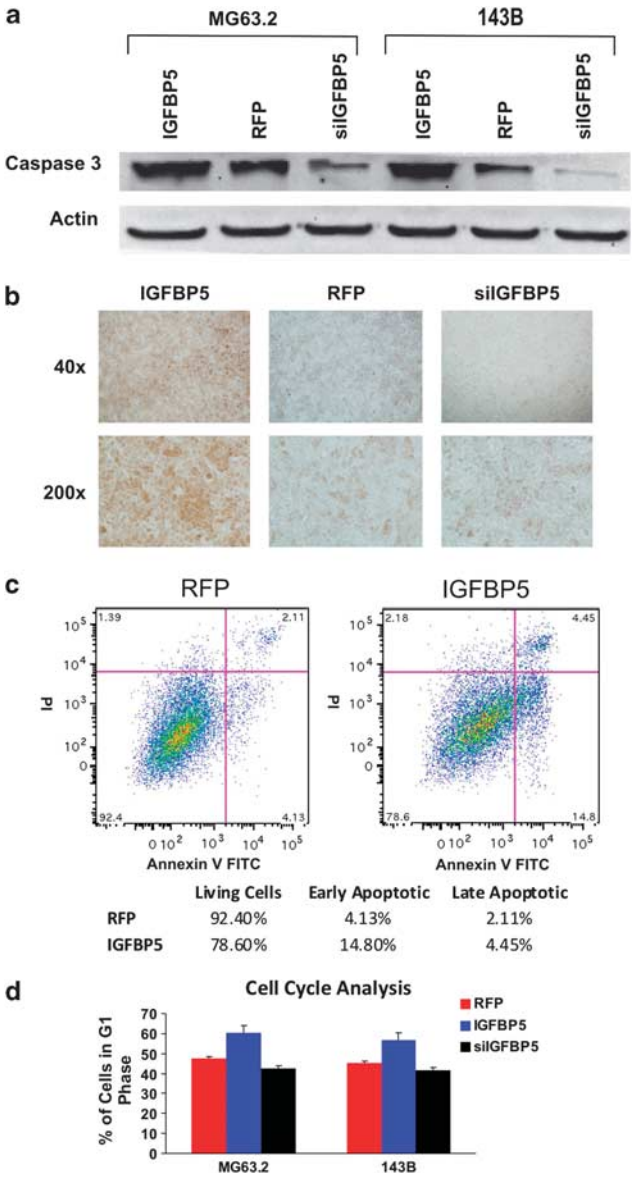

Figure 6 IGFBP5 induces apoptosis, whereas IGFBP5 knockdown promotes proliferation. (**a**) Western blot using an anti-caspase-3 antibody in the 143B and MG63.2 cell lines expressing RFP control, IGFBP5 or siIGFBP5. (**b**) Immunohistochemistry staining for caspase-3 in each treatment group in 143B cell lines. Note the increased staining in the IGFBP5 group. (**c**) Apoptosis analysis by flow cytometry for MG63.2 cell lines expressing RFP control of IGFBP5. The cells were clustered according to those undergoing early and late phases of apoptosis. (**d**) Cell cycle analysis by flow cytometry of each treatment group for 143B and MG63.2 cell lines. The percentage of cells in the G1 phase is shown.

suppression of OS cell proliferation and promotion of apoptosis (Schneider *et al*., 2001; Akkiprik *et al*., 2008). IGFBP5 has been shown to traffic into the nucleus (Schedlich *et al*., 2000) and interact with transcription factors such as four-and-a-half LIM protein in U2 human OS cells, which can have downstream effects on tumor growth and metastasis (Amaar *et al*., 2002). In fact, nuclear localization of IGFBP5 has been associated with apoptosis in breast cancer (Butt *et al*., 2003; Butt *et al*., 2005) and inhibition of cell proliferation in murine OS/50-K8 OS cells (Schneider *et al*., 2001).

In summary, we have identified IGFBP5 as a novel protein in the pathogenesis and metastasis of OS. We have demonstrated that IGFBP5 inhibits phenotypes important for OS growth and metastasis. As IGFBP5 is a secreted protein, its potential therapeutic applications can easily be translated to the clinical arena.

Materials and methods

Tissue culture

HEK293 and human OS lines MG63, 143B, MNG/HOS and TE85 were purchased from ATCC (Manassas, VA, USA). We also used MG63.2, a highly tumorigenic line derived from the metastasis of parental MG63, as previously reported (Su *et al*., 2009). Cells were maintained in complete Dulbecco's modified Eagle's media containing 10% fetal bovine serum (HyClone,

Logan, UT, USA), 1 mmol/l sodium pyruvate, 100 units of penicillin and 100 μg of streptomycin at 37 °C in 5% CO_2.

Recombinant adenoviral vectors expressing IGFBP5 and siIGFBP5

The cDNA coding region to human IGFBP5 was PCR amplified and subcloned into the adenoviral shuttle vector pAdTrace-TO4 (He *et al*., 1998; Kang *et al*., 2004; Luo *et al*., 2007a; Kang *et al*., 2009). The siRNA-knockdown oligo cassettes were cloned into the shuttle vector pSES system (Luo *et al*., 2007b; Luo *et al*., 2008). The siIGFBP5 and scrambled siRNA control sequences were generated using the siDesign software from www.dharmacon.com/designcenter. Cloning details and oligo sequences are available upon request. Recombinant adenovirus generation was carried out using the AdEasy system, as previously described (He *et al*., 1998; Kang *et al*., 2004; Luo *et al*., 2007a; Kang *et al*., 2009). Adenoviruses were produced in HEK293 cells and amplified to obtain high titers (He *et al*., 1998; Kang *et al*., 2004; Luo *et al*., 2008), resulting in the adenoviruses expressing IGFBP5 (AdR-IGFBP5) and siIGFBP5 (AdR-siIGFBP5) that also expressed RFP as a marker to monitor infection efficiency. AdRFP was used as a control.

Microarray analysis

The microarray analysis was performed at the University of Chicago Functional Genomics Core Facility, as previously described (Tusher *et al*., 2001). Briefly, we first used fully characterized total RNA samples, which were isolated from cells, primary tumors and metastatic tumors, for target preparation, and subjected them to hybridizations to the Affymetrix genechip (Affymetrix, Santa Clara, CA, USA). Target preparation protocol was provided by the Affymetrix GeneChip Expression Analysis Manual. We used DNA-Chip hierarchical cluster analysis and Significance Analysis of Microarrays, as previously described (Tusher *et al*., 2001). The model-based approach allowed probe-level analysis and facilitated automatic probe selection in the analysis stage to reduce errors caused by outliers, cross hybridizing probes and image contamination. The default clustering algorithm of genes was used for the DNA-Chip analysis. Briefly, the distance between two genes was defined as $1-r$, where r is the Pearson's correlation coefficient between the standardized expression values (make mean 0 and standard deviation 1) of the two genes. Two genes with the closest distance were first merged into a supergene and connected by branches with length representing their distance. The expression values of the newly formed supergene were the average of standardized expression values of the two genes across samples. Then the next pair of genes (supergenes) with the smallest distance was chosen to merge and the process was repeated *n–1* times to merge all the *n* genes.

RNA isolation and semi-quantitative RT–PCR

Using TRIZOL Reagents (Invitrogen, Carlsbad, CA, USA), we isolated total RNA and generated cDNA templates via RT–PCR. The cDNA products were used for semi-quantitative PCR templates, as described previously (Luu *et al*., 2005a; Luo *et al*., 2008; Sharff *et al*., 2009; Su *et al*., 2009). All samples were normalized by the GADPH expression level. Primer sequences are available upon request.

Western blot analysis for IGFBP5 and caspase-3 expression

Western blot analysis was performed as described (Luu *et al*., 2005b; Luo *et al*., 2008). For all overexpression and knockdown experiments, subconfluent cells were infected with AdRFP, AdR-IGFBP5 or AdR-siIGFBP5. Whole cell lysates were used. Anti-IGFBP5 or anti-caspase-3 antibodies were purchased from Santa Cruz Biotechnology (Santa Cruz, CA, USA) and secondary antibodies conjugated with horseradish peroxidase from Pierce (Rockford, IL, USA).

Cell proliferation assay

Cell proliferation assays were performed as previously described (Luu *et al*., 2005a). Briefly, subconfluent tumor cells were infected with control AdRFP, AdR-IGFBP5 or AdR-siIGFBP5 and replated at 72 h in 1% fetal bovine serum complete media. The cells were then collected by trypsinization at the indicated time point and viable cells were counted. Each assay was done in triplicate.

Matrigel invasion assay

Matrigel cell invasion assays were performed as described Su *et al*., 2009). Briefly, subconfluent tumor cells were infected with control AdRFP, AdR-IGFBP5 or AdR-siIGFBP5 and assayed at 72 h. The membranes containing the invading cells were fixed in 10% formalin, stained with hematoxylin, unmigrated cells removed and mounted onto slides with Permount. Four random high power fields ($\times 200$) were counted per insert and representative images were obtained. The assay was performed in triplicate.

Wound healing cell migration assay

Wound healing migration assays were performed as previously described (Luu *et al*., 2005b; Luo *et al*., 2008). Subconfluent cells were infected with AdRFP, AdR-IGFBP5 or AdR-siIGFBP5. After 72 h, the cells were trypsinized, counted and re-plated in 1% fetal bovine serum complete media in six-well dishes containing a sterile metal three-pronged cross (0.75 mm thick) to create a consistent gap in the monolayer of cells. At 12 h after plating, the cross was removed. Bright-field images of the field adjacent to the left center arm of the cross were taken at 0, 12, 24 and 36 h, after removing the cross to assess cell migration across the gap. These assays were done in triplicate.

Caspase-3 immunohistochemical staining

Immunohistochemical staining was carried out as described (Luo *et al*., 2004; Peng *et al*., 2004). Briefly, subconfluent cells were infected with AdRFP, AdR-IGFBP5 or AdR-siIGFBP5 and stained at 72 h. The fixed cells were blocked with bovine serum, avidin and biotin blocking solution. Cells were probed with an anti-cleaved caspase-3 antibody, followed by incubation with anti-goat IgG secondary antibody conjugated with horseradish peroxidase (Pierce).

Flow cytometry

Subconfluent cells were infected with AdRFP, AdR-IGFBP5 or AdR-siIGFBP5. After 72 h, the cells were trypsinized and re-plated at subconfluent conditions. Cells were harvested at 48 h, fixed with 70% ethanol, washed with phosphate-buffered saline and stained with propidium iodide. Cells were sorted and analyzed according to phase of cell cycle. Additionally, cells in the early- and late phases of apoptosis were sorted with propidium iodide and annexin V.

Orthotopic xenograft model

Two highly tumorigenic and metastatic cell lines, MG63.2 and 143B, with stable expression of luciferase were infected with AdRFP, AdR-IGFBP5 or AdR-siIGFBP. At 36 h post infection, cells were harvested and prepared for injections (1.5×10^6/injection) into the proximal posterior tibia of athymic nude mice (male, Harlan Sprague Dawley, 4–6 weeks old) as previously described, except for a subperiosteal injection

(Luo *et al*., 2008; Su *et al*., 2009). Although the subperiosteal injection has a lower metastatic efficiency compared with our previously described intratibial injection (Luo *et al*., 2008; Su *et al*., 2009), we now use the subperiosteal injection to avoid the immediate 10% mortality associated with the intratibial injections from marrow embolic events. This approach reduced our animal cost, as well as animal mortality. We used five mice per group, repeating the experiments in two separate batches. Tumors were measured every 3–4 days and the tumor volume and doubling time were calculated, as previously reported (Luu *et al*., 1998). At 4 weeks after implantation for 143B cells, and 8 weeks for MG63.2 cells, animals were killed. Primary tumors and lungs were harvested for evaluation.

Xenogen bioluminescence imaging
Bioluminescent imaging was performed, as previously described, using the Xenogen IVIS 200 imaging system (Luo *et al*., 2008; Su *et al*., 2009). The animals were injected intraperitoneally with a D-Luciferin sodium salt (Gold BioTechnology, St Louis, MO, USA) at 100 mg/kg in 0.1 ml sterile phosphate-buffered saline. The pseudoimages were obtained by superimposing the emitted light over the gray-scale photographs of the animal. Quantitative analysis was done with Xenogen's Living Image V2.50.1 software as described (Luo *et al*., 2008; Su *et al*., 2009).

Animal histologic evaluation
Histologic evaluation was performed as previously described (Su *et al*., 2009). All samples were assigned a number and the treatment group blinded. The harvested tumors and lungs were fixed with 10% formalin, embedded in paraffin, serially sectioned and stained with hematoxylin and eosin. Evaluation of the histologic slides was performed by a blinded, trained pathologist.

MicroCT imaging
MicroCT imaging was performed as previously described (Kang *et al*., 2009). The harvested tumors were fixed in 10% formalin and subjected to imaging. After the imaging, the data was analyzed via the Amira software program (Visage Imaging, San Diego, CA, USA).

Patient sample tissue array and immunohistochemistry
The pathology database was searched for pulmonary metastatic OS under an approved Institutional Review Board protocol. A total of 25 patients with pulmonary metastectomies were identified. In all, 14 chemotherapy-naive biopsy specimens matching to 14 of the 25 patients with metastatic lesions were identified in the pathology database; 11 of the 25 patients did not have their biopsies at our institution or missing blocks and therefore, the paraffin blocks for those primary samples were not available. In patients who had multiple pulmonary metastectomies (that is, multiple pulmonary metastases), all the metastatic specimens were included and immunohistochemical scores averaged. The samples were collected from patients treated between 1986 and 2009. Tissue arrays containing primary and metastatic OS specimens were generated by The University of Chicago Pathology Core Facility. The slides were retrieved and reviewed by a board-certified musculoskeletal pathologist. The paraffin blocks were retrieved, cores identified by the pathologist and the tissue array created by the Core Facility. Two core plugs (1 mm) per sample were collected for the array. The tissue array blocks were sectioned and unstained slides subjected to immunohistochemical staining. Anti-IGFBP5 antibodies were purchased from Santa Cruz Biotechnology (Santa Cruz) and secondary antibodies conjugated with horseradish peroxidase from Pierce. Immunohistochemical staining and scoring of the staining intensity was performed as previously described (Luu *et al*., 2005b) and blinded to any clinical data. Briefly, staining score was rated as 0 (no staining), 1+ (weak), 2+ (moderate) or 3+ (strong). Staining score 0 was defined as no staining visible; 1+ was defined light staining requiring high power magnification ($\times 200$) to identify the staining pattern; 2+ was defined as moderate staining requiring medium power magnification ($\times 100$) to identify the staining pattern; 3+ was defined as dark staining visible at low power magnification ($\times 40$).

Statistical analysis
A two-tailed Student's *t*-test was used to compare the expression of IGFBP5 (quantitative RT–PCR) between the parental MG63 and the MG63.2 lines, as well as comparing the IGFBP5 and siIGFBP5 groups with the RFP control for the Matrigel invasion assay, tumor doubling time, cell proliferation and cell cycle analysis. The immunohistochemical staining scores for the matched patient samples were compared using the Paired Signed Rank test. A two sample Wilcoxon Rank-Sum test (Mann–Whitney) was used to compare the immunohistochemical scores for all primary and metastatic samples. A χ^2-test was used to analyze the presence of lung metastasis in both the MG63.2 and 143B cell lines.

Conflict of Interest

The authors declare no conflict of interest.

Acknowledgements

We thank Dr Xinmin Li, PhD (Director of The UCLA Clinical Microarray Core) for his help with the microarray and cluster analysis. We also sincerely thank Dr Anthony Montag, Leslie Martin and Guarav Luther for the creation of the tissue array. We also thank Dr Theodore Karrison for help with the statistical analysis. This work was supported in part by research grants from The American Cancer Society (HHL and TCH), the Brinson Foundation (HHL, TCH, RCH), The National Institute of Health (HHL, TCH, RCH), the Orthopaedic Research and Education Foundation (HHL, RCH), the Natural Science Foundation of China (#81001197 to YS), and the 973 Program of the Ministry of Science and Technology of China (#2011CB707906 to JL and TCH).

References

Akkiprik M, Feng Y, Wang H, Chen K, Hu L, Sahin A *et al*. (2008). Multifunctional roles of insulin-like growth factor binding protein 5 in breast cancer. *Breast Cancer Res* **10**: 212.

Amaar YG, Thompson GR, Linkhart TA, Chen ST, Baylink DJ, Mohan S. (2002). Insulin-like growth factor-binding protein 5 (IGFBP-5) interacts with a four and a half LIM protein 2 (FHL2). *J Biol Chem* **277**: 12053–12060.

Avnet S, Sciacca L, Salerno M, Gancitano G, Cassarino MF, Longhi A *et al*. (2009). Insulin receptor isoform A and insulin-like growth factor II as additional treatment targets in human osteosarcoma. *Cancer Res* **69**: 2443–2452.

Butt AJ, Dickson KA, Jambazov S, Baxter RC. (2005). Enhancement of tumor necrosis factor-alpha-induced growth inhibition by insulin-like growth factor-binding protein-5 (IGFBP-5), but not

IGFBP-3 in human breast cancer cells. *Endocrinology* **146**: 3113–3122.

Butt AJ, Dickson KA, McDougall F, Baxter RC. (2003). Insulin-like growth factor-binding protein-5 inhibits the growth of human breast cancer cells *in vitro* and *in vivo*. *J Biol Chem* **278**: 29676–29685.

Cheung C, Vesey D, Cotterill A, Douglas M, Gobe G, Nicol D *et al*. (2005). Altered messenger RNA and protein expressions for insulin-like growth factor family members in clear cell and papillary renal cell carcinomas. *Int J Urol* **12**: 17–28.

Davis AM, Bell RS, Goodwin PJ. (1994). Prognostic factors in osteosarcoma: a critical review. *J Clin Oncol* **12**: 423–431.

Fuchs B, Pritchard DJ. (2002). Etiology of osteosarcoma. *Clin Orthop* **397**: 40–52.

He TC, Zhou S, da Costa LT, Yu J, Kinzler KW, Vogelstein B. (1998). A simplified system for generating recombinant adenoviruses. *Proc Natl Acad Sci USA* **95**: 2509–2514.

Kang Q, Song WX, Luo Q, Tang N, Luo J, Luo X *et al*. (2009). A comprehensive analysis of the dual roles of BMPs in regulating adipogenic and osteogenic differentiation of mesenchymal progenitor cells. *Stem Cells Dev* **18**: 545–559.

Kang Q, Sun MH, Cheng H, Peng Y, Montag AG, Deyrup AT *et al*. (2004). Characterization of the distinct orthotopic bone-forming activity of 14 BMPs using recombinant adenovirus-mediated gene delivery. *Gene Ther* **11**: 1312–1320.

Kaste SC, Pratt CB, Cain AM, Jones-Wallace DJ, Rao BN. (1999). Metastases detected at the time of diagnosis of primary pediatric extremity osteosarcoma at diagnosis: imaging features. *Cancer* **86**: 1602–1608.

Letson GD, Muro-Cacho CA. (2001). Genetic and molecular abnormalities in tumors of the bone and soft tissues. *Cancer Control* **8**: 239–251.

Luo J, Deng ZL, Luo X, Tang N, Song WX, Chen J *et al*. (2007a). A protocol for rapid generation of recombinant adenoviruses using the AdEasy system. *Nat Protoc* **2**: 1236–1247.

Luo Q, Kang Q, Si W, Jiang W, Park JK, Peng Y *et al*. (2004). Connective tissue growth factor (CTGF) is regulated by Wnt and bone morphogenetic proteins signaling in osteoblast differentiation of mesenchymal stem cells. *J Biol Chem* **279**: 55958–55968.

Luo Q, Kang Q, Song WX, Luu HH, Luo X, An N *et al*. (2007b). Selection and validation of optimal siRNA target sites for RNAi-mediated gene silencing. *Gene* **395**: 160–169.

Luo X, Sharff KA, Chen J, He TC, Luu HH. (2008). S100A6 expression and function in human osteosarcoma. *Clin Orthop Relat Res* **466**: 2060–2070.

Luu HH, Kang Q, Park JK, Si W, Luo Q, Jiang W *et al*. (2005a). An orthotopic model of human osteosarcoma growth and spontaneous pulmonary metastasis. *Clin Exp Metastasis* **22**: 319–329.

Luu HH, Zagaja GP, Dubauskas Z, Chen SL, Smith RC, Watabe K *et al*. (1998). Identification of a novel metastasis-suppressor region on human chromosome 12. *Cancer Res* **58**: 3561–3565.

Luu HH, Zhou L, Haydon RC, Deyrup AT, Montag AG, Huo D *et al*. (2005b). Increased expression of S100A6 is associated with decreased metastasis and inhibition of cell migration and anchorage independent growth in human osteosarcoma. *Cancer Lett* **229**: 135–148.

Manara MC, Landuzzi L, Nanni P, Nicoletti G, Zambelli D, Lollini PL *et al*. (2007). Preclinical *in vivo* study of new insulin-like growth factor-I receptor–specific inhibitor in Ewing's sarcoma. *Clin Cancer Res* **13**: 1322–1330.

Mankin HJ, Hornicek FJ, Rosenberg AE, Harmon DC, Gebhardt MC. (2004). Survival data for 648 patients with osteosarcoma treated at one institution. *Clin Orthop* **429**: 286–291.

Mukherjee A, Rotwein P. (2007). Insulin-like growth factor binding protein-5 in osteogenesis: facilitator or inhibitor? *Growth Horm IGF Res* **17**: 179–185.

Peng Y, Kang Q, Luo Q, Jiang W, Si W, Liu BA *et al*. (2004). Inhibitor of DNA binding/differentiation helix-loop-helix proteins mediate bone morphogenetic protein-induced osteoblast differentiation of mesenchymal stem cells. *J Biol Chem* **279**: 32941–32949.

Ragland BD, Bell WC, Lopez RR, Siegal GP. (2002). Cytogenetics and molecular biology of osteosarcoma. *Lab Invest* **82**: 365–373.

Rosenzweig SA. (2004). What's new in the IGF-binding proteins? *Growth Horm IGF Res* **14**: 329–336.

Schedlich LJ, Le Page SL, Firth SM, Briggs LJ, Jans DA, Baxter RC. (2000). Nuclear import of insulin-like growth factor-binding protein-3 and -5 is mediated by the importin beta subunit. *J Biol Chem* **275**: 23462–23470.

Schneider MR, Wolf E, Hoeflich A, Lahm H. (2002). IGF-binding protein-5: flexible player in the IGF system and effector on its own. *J Endocrinol* **172**: 423–440.

Schneider MR, Zhou R, Hoeflich A, Krebs O, Schmidt J, Mohan S *et al*. (2001). Insulin-like growth factor-binding protein-5 inhibits growth and induces differentiation of mouse osteosarcoma cells. *Biochem Biophys Res Commun* **288**: 435–442.

Sharff KA, Song WX, Luo X, Tang N, Luo J, Chen J *et al*. (2009). Hey1 basic helix-loop-helix protein plays an important role in mediating BMP9-induced osteogenic differentiation of mesenchymal progenitor cells. *J Biol Chem* **284**: 649–659.

Song H, Shand JH, Beattie J, Flint DJ, Allan GJ. (2001). The carboxy-terminal domain of IGF-binding protein-5 inhibits heparin binding to a site in the central domain. *J Mol Endocrinol* **26**: 229–239.

Stolf BS, Carvalho AF, Martins WK, Runza FB, Brun M, Hirata Jr R *et al*. (2003). Differential expression of IGFBP-5 and two human ESTs in thyroid glands with goiter, adenoma and papillary or follicular carcinomas. *Cancer Lett* **191**: 193–202.

Su Y, Luo X, He BC, Wang Y, Chen L, Zuo GW *et al*. (2009). Establishment and characterization of a new highly metastatic human osteosarcoma cell line. *Clin Exp Metastasis* **26**: 599–610.

Takahashi M, Papavero V, Yuhas J, Kort E, Kanayama HO, Kagawa S *et al*. (2005). Altered expression of members of the IGF-axis in clear cell renal cell carcinoma. *Int J Oncol* **26**: 923–931.

Tusher VG, Tibshirani R, Chu G. (2001). Significance analysis of microarrays applied to the ionizing radiation response. *Proc Natl Acad Sci USA* **98**: 5116–5121.

Wang H, Rosen DG, Fuller GN, Zhang W, Liu J. (2006). Insulin-like growth factor-binding protein 2 and 5 are differentially regulated in ovarian cancer of different histologic types. *Mod Pathol* **19**: 1149–1156.

Whelan JS. (1997). Osteosarcoma. *Eur J Cancer* **33**: 1611–1618; discussion 1618–9.

Xu C, Graf LF, Fazli L, Coleman IM, Mauldin DE, Li D *et al*. (2007). Regulation of global gene expression in the bone marrow microenvironment by androgen: androgen ablation increases insulin-like growth factor binding protein-5 expression. *Prostate* **67**: 1621–1629.

Yonemoto T, Tatezaki S, Ishii T, Satoh T, Kimura H, Iwai N. (1998). Prognosis of osteosarcoma with pulmonary metastases at initial presentation is not dismal. *Clin Orthop* **349**: 194–199.